Satellite observations of modulation of surface winds by typhoon-induced upper ocean cooling

I.-I. Lin,[1] W. Timothy Liu,[2] Chun-Chieh Wu,[3] J. C. H. Chiang,[4,5] and Chung-Hsiung Sui[6]

Received 14 June 2002; accepted 15 August 2002; published 12 February 2003.

[1] Two remote sensing data sets, the Tropical Rainfall Measurement Mission Sea Surface Temperature (SST) and the NASA QuikSCAT ocean surface wind vectors, are analysed to study ocean-atmosphere interactions in cold SST regions formed in the trail of two typhoon events. Anomalously cold SST patches up to 6°C below the surrounding warm tropical ocean SST are found along the trail of typhoon tracks as cold, deep waters are entrained up to the mixed layer due to typhoon forcing. In both typhoon events, significant and systematic weakening of surface wind speed is found over cold SST patches relative to surface wind speed in surrounding regions. The wind speed anomalies disappear as the patches recover to the level of the surrounding SST. The results are consistent with the mechanism proposed by Wallace et al. that surface winds are modulated by SST via stability. As wind within the well-mixed boundary layer moves over the cold patch, boundary layer stability increases, vertical mixing is suppressed, and the vertical wind shear increases; reduction in surface wind speed is caused. In particular, our result shows that this mechanism can act on relatively small spatial (≈100 *km*) and short (≈1 *day*) time scales. *INDEX TERMS:* 3360 Meteorology and Atmospheric Dynamics: Remote sensing; 3339 Meteorology and Atmospheric Dynamics: Ocean/atmosphere interactions (0312, 4504); 3307 Meteorology and Atmospheric Dynamics: Boundary layer processes. **Citation:** Lin, I.-I., W. T. Liu, C.-C. Wu, J. C. H. Chiang, and C.-H. Sui, Satellite observations of modulation of surface winds by typhoon-induced upper ocean cooling, *Geophys. Res. Lett.*, *30*(3), 1131, doi:10.1029/2002GL015674, 2003.

1. Introduction

[2] Tropical cyclones (typhoons) are formed in tropical oceans whereby the energy of typhoons is supplied by ocean through surface fluxes [*Emanuel*, 1986]. The ocean in turn responds to typhoon forcing; a prominent feature of which is the cold Sea Surface Temperature (SST) patches at the trail of typhoons [*Leipper*, 1967; *Price*, 1981; *Nelson*, 1996; *Monaldo et al.*, 1997; *Wentz et al.*, 2000]. Such cold patches are primarily the results of typhoon-induced vertical entrainment of deep cold waters up to the ocean mixed layer. These cold patches may be as much as 5–6 degree centigrade cooler than the surrounding warm SST [*Wentz et al.*, 2000]. As such, they represent sizable perturbations of the SST in an otherwise relatively uniform warm ocean environment, and present a unique natural experiment to investigate the nature of ocean-atmosphere interaction. In this work, nearest co-incident/co-located wind vectors from the NASA QuikSCAT and the cloud-penetrating SST data from the Tropical Rainfall Measuring Mission (TRMM) Microwave Imager (TMI) are analysed to study the relationship between surface winds and SST after 2 recent typhoon episodes in the Western Pacific Ocean (WPO) and the South China Sea (SCS).

2. Typhoon Cases

[3] The two typhoon cases investigated are Kai-Tak and Bilis. Kai-Tak was a moderate category 2 typhoon in the Saffir-Simpson hurricane scale. It traveled relatively slowly (0–1.4 m/s) on the northern part of the SCS from 5 to 8 July 2000, then moved rapidly (6.1 m/s) northwards on 12:00 UTC 8 July. A distinct cold patch is observed in the TMI/SST image on 9 July, immediately after Kai-Tak's departure. The temperature at the centre of the patch was 21.8°C, more than 6°C colder than the surrounding SST of 28.2°C. The SST in the patch slowly recovered to the level of the surrounding SST over a period of 10 days. Details of the SST evolution are described in *Lin et al.* [in preparation].

[4] Bilis was a category 4 typhoon. It traveled at around 6.1 m/s from southeast to northwest in the WPO from 19 to 22 August 2000, hit southern Taiwan, and then proceeded to the Taiwan Strait on 23 August. Due to variation in typhoon intensity and local hydrological conditions (e.g., mixed layer thickness and vertical distribution of temperature), the cold patch induced by Bilis is found most evidently between 123–127°E, 19–25°N (see section 4). The minimum SST in the cold patch is 25.8°C and the surrounding SST is around 29.5–30.5°C. This cold patch recovered more rapidly than Kai-Tak's, by 26 August, the SST has recovered back to 30.0°C. Details are given in *Lin et al.* [in preparation].

3. Ocean-Atmosphere Interaction Following Typhoon Kai-Tak

[5] Figure 1 illustrates the representative SST images before and after typhoon Kai-Tak passed through the region; the corresponding QuikSCAT images are depicted in Figure 2. Matching QuikSCAT wind vectors are overlaid on the SST images (Figure 1) and contours of the matching SST data are overlaid on the wind speed images (Figure 2). Prior to Kai- Tak's arrival, the northern SCS was under typical summer conditions [*Chu et al.*, 1997] as

[1]National Center for Ocean Research, Taipei, Taiwan.
[2]Jet Propulsion Laboratory, NASA, USA.
[3]Department of Atmospheric Science, National Taiwan University, Taiwan.
[4]Joint Institute for the Study of the Atmosphere and Ocean, University of Washington, USA.
[5]Department of Geography, University of California, Berkeley, USA.
[6]Institute of Hydrological Sciences, National Central University, Taiwan.

0094-8276/03/2002GL015674$05.00

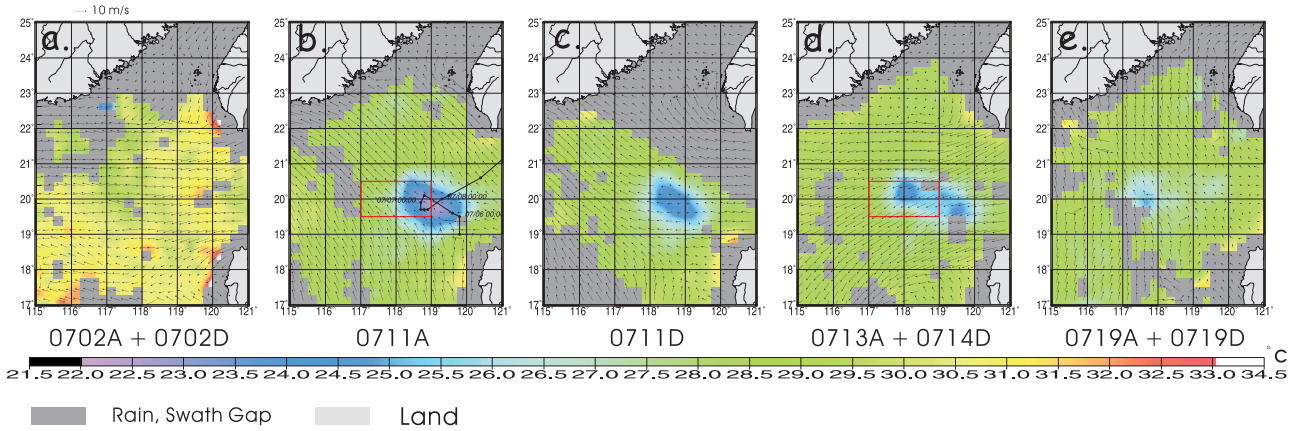

Figure 1. Sequence of representative TMI/SST images showing the evolution of Kai-Tak typhoon's cold SST patch, (a) before typhoon on 2 July 2000, composite image of 2 passes at 05:30 UTC and 13:36 UTC; (b) after typhoon on 11 July, ascending pass at 1:06 UTC; (c) descending pass at 09:12 UTC 11 July; (d) composite of 0:18 UTC 13 July and 23:06 UTC 14 July passes; (e) composite of 04:18 UTC and 20:36 UTC 19 July passes. Matching QuikSCAT wind vectors are overlaid. The trajectory of Kai-Tak is depicted in Figure 1b. Kai-Tak's location at 00U TC 6 July is at 119.8°E, 19.5°N; at 00 UTC 7 July, 118.7°E, 19.9°N; at 00U TC 8 July, 119.3°E, 20.0°N.

represented by the composite image (Figure 1a) of the two TMI passes (ascending pass at 05:30 UTC and descending pass at 13:36 UTC) on 2 July. The SST is in the range of 30.5–33.0°C. The corresponding surface wind field (Figure 2a) shows higher- wind speed (9–11 m/s) in the region north of 19°N, and lower wind speed south of 19°N (3–6 m/s). No evident association between SST and wind is observed. Kai-Tak passed the SCS between 12:00 UTC 5 July and 12:00 UTC 8 July. Its trajectory is shown in Figure 1b. The maximum SST cooling occurred on 9 July. However, because the wind fields were still then under the influence of the typhoon, we analyse data starting 11 July. Figure 1b (acquisition time: 1:06 UTC, 11 July) shows the Kai-Tak-induced cold patch. This cold SST patch (118–120°E, 19–21°N) has the dimension of around 150–200 km, comparable to Kai-Tak's 150km Radius of Maximum Wind (RMW). The minimum SST of 22.7°C is found (colour coded: purple) in the centre (118.9°E, 19.9°N) of the oval cold patch and increases outwards to 26°C (light blue) towards the edge. The surrounding SST is around 29–30°C (dark-light green). The corresponding wind field (Figure 2b, acquisition time 21:48 UTC 10 July) shows a distinctive minimum co-located with the cold patch. The wind speed inside the cold patch is between 2.5 to 6m/s (dark purple-light blue) while the surrounding wind speed is between 8–11m/s (green-yellow colour).

[6] To quantify the relationship between SST and wind speed, data from a representative band (117–119°E, 19.5–20.5°N, location depicted in Figure 1b) crossing from the ambient to the oval feature is extracted in both SST and wind speed images (Figures 1b and 2b). Figure 3 illustrates the latitudinal band average (19.5–20.5°N) of SST and wind speed along 117–119°E longitude. A positive correlation between SST and wind speed is seen, from 9.8 m/s at the edge of the cold patch (28.8°C) to 4 m/s at the center (23.4°C). The correlation coefficient is 0.94. The positive correlation between SST and wind speed persisted for 8 days, till 19 July. For example, Figures 1c and 2c shows the SST and wind speed distribution, respectively, 8 hours after the image in Figure 1b. The association between SST and

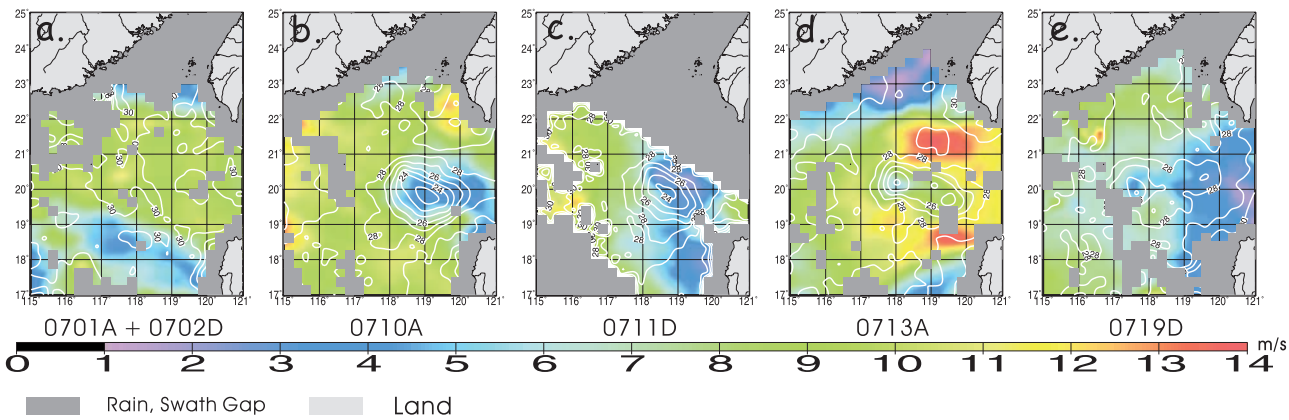

Figure 2. Matching (with Figure 1) QuikSCAT wind speed image with TMI/SST contours overlay showing association between SST and wind speed after typhoon passage, (a) before typhoon, composite image of 22:13 UTC 1 July 2000 and 10:42 UTC 2 July passes; (b) after typhoon at 21:48 UTC 10 July; (c) 10:09 UTC 11 July; (d) 22:11 UTC, 13 July; (e) 10:10 UTC, 19 July.

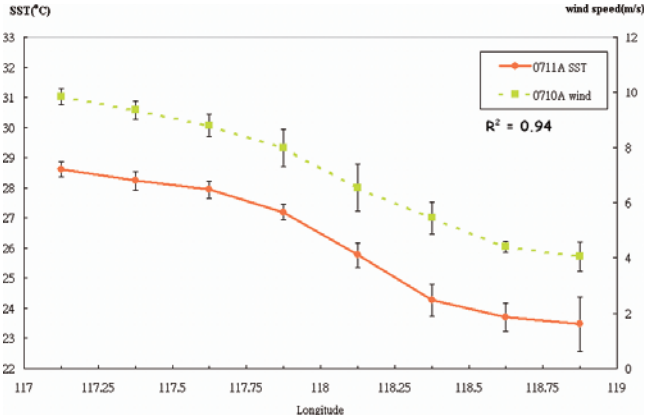

Figure 3. Scatter plot of wind speed vs. SST for data averaged across the latitudinal band of 19.5–20.5°N. The band location is depicted in Figure 1b.

wind speed in the cold patch region (118–120°E, 19–21°N) is still clearly evident. The low wind patch at the south of the cold patch (i.e., 118–120°E, 17–19°N) in Figure 2c, however, is not found to be associated with the cold patch and may be related to synoptic variability. It appears to be transient and is neither found in the images before (Figure 2b) nor after (Figure 2d). By 13 July, the SST pattern had weakened and elongated (Figure 1d). The corresponding wind speed (Figure 2d) evolved similarly, again illustrating the close-association between SST and wind. This occurs despite the fact that the wind speed north and south of the cold patch is relatively high (≥12 m/s) on 13 July. This highlights the systematic lowering of wind speed over the SST patch independent of the significant synoptic variability evident in surface wind over the surrounding region. The SST-wind correlation for 13 July is similarly demonstrated in the latitudinal band average (19.5–20.5°N, location depicted in Figure 1d) of SST and wind speed distribution along the 117–119°E longitude with correlation coefficient = 0.57 (not shown).

[7] On 19 July, the cold patch is reduced to a small circular feature at around 117.5°E, 20°N (Figure 1e), and disappears shortly thereafter. The minimum SST is around 25.5°C. Over this low SST patch, a low wind speed patch of similar size and shape (117–118°E, 19.8–20.7°N is seen (Figure 2e).

4. Ocean-Atmosphere Interaction Following Typhoon Bilis

[8] We found similar association between SST and wind in the cold SST patch generated by typhoon Bilis. No association between SST and wind speed is apparent before the passage of Bilis (not shown). After Bilis passed, on 24 August, a cold patch (123–127°E, 19–25°N) is visible to the right following the typhoon track (Figure 4b). The mechanism accounting for such right-bias of the cold patch has been well-investigated [*Chang and Anthes*, 1978; *Price*, 1981]. In the cold patch, the SST is in the range of 25.5–27.0°C (purple-blue) in contrast to the ambient SST of above 29°C (green). Figure 4b illustrates the corresponding wind speed image. A low wind speed patch (124–128°E, 19–25°N) is found co-located with the patch. The correlation (correlation coefficient = 0.84) between SST and wind speed is seen clearly in the latitudinal band (location depicted in Figure 4a) average (20–21°N) of the respective data along the 124–130°E longitude (not shown).

[9] The positive correlation between SST and wind speed shown in the 3 bands from Figures 1b, 1d, and 4a suggests that there may be a more general relationship between changes of wind speed with changes of SST. By subtracting the ambient SST and wind speed outside the SST patch from the data points of the 3 bands in Figures 1b, 1d, and 4a, an anomaly SST.vs. wind speed scatter diagram is obtained (Figure 5). The 3 groups of data follow similar slopes; typically a 1 degree SST reduction is equivalent to a 1.0 m/s decrease in wind speed. The correlation coefficient, taken all points plotted in Figure 5, is 0.82.

5. Discussion and Conclusion

[10] The fact that a similar relationship between SST and wind is found for the two cases argues for a common physical mechanism that closely links surface winds to SST. Our results appears consistent with the mechanism proposed by *Wallace et al.* [1989]. They proposed that SST is coupled to

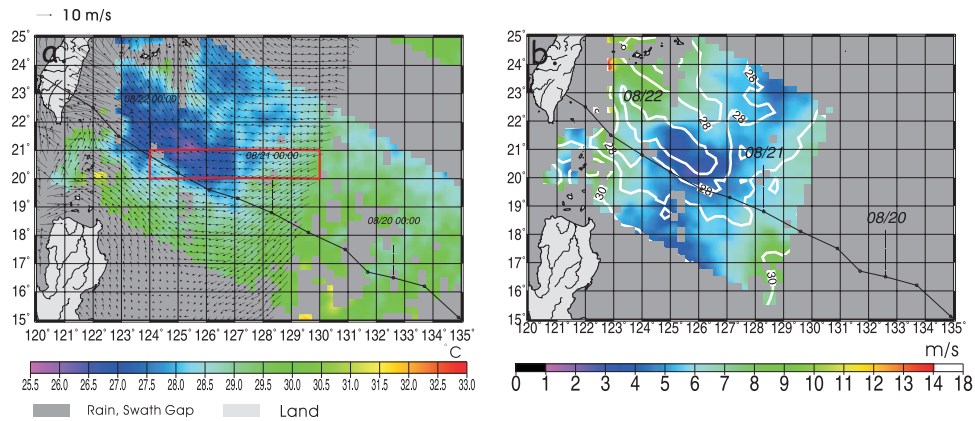

Figure 4. (a) Same as Figure 1 but for Bilis's case showing TMI/SST images after a Bilis' passage on 09:24 UTC 24 August. (b) Same as Figure 2 but for Bilis's case showing matching (with Figure 4a) QuikSCAT wind speed image after Bilis' passage at 10:04 UTC 24 August.

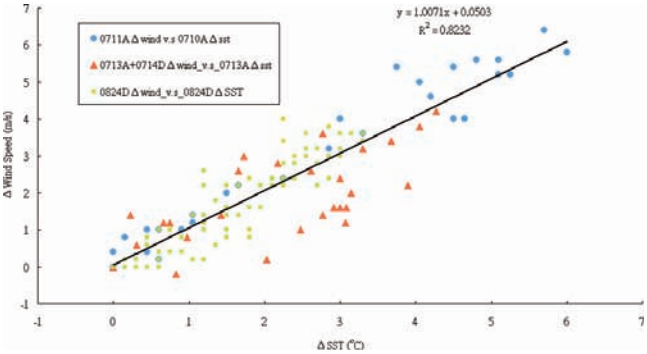

Figure 5. Scatter plot of wind speed anomalies vs. SST anomalies, showing consistent correlation for the 3 bands of data from Figures 1b, 1d, and 4a.

surface wind through changes in the atmospheric boundary layer stability. Over colder waters, the marine boundary layer is stable, vertical mixing is suppressed, and vertical wind shear increases, the surface wind speed is reduced.

[11] Recent studies [*Xie et al.*, 1998; *Liu et al.*, 2000; *Wentz et al.*, 2000; *Chelton et al.*, 2001; *Xie et al.*, 2001] of the SST-wind relationship in the case of Tropical Instability Waves (TIWs) and the Eastern Pacific Ocean cold tongue have demonstrated the mechanism for surface wind-SST interaction as proposed by *Wallace et al.* [1989]. Our results supports the *Wallace et al.* [1989] hypothesis in the SST-wind interaction in a different situation, namely in the cold SST patches of typhoons. What we show in our example that is not shown in the previous studies is the small space and short time scales over which that this mechanism can act. In *Chelton et al.* [2001], the time and space scales are typical of tropical instability waves, i.e., ≈20 days to 40 days and ≈1000 to 2000 km. In the typhoon-induced cold SST patch situation, the impact of SST on surface winds manifests itself on the order of a day and of the spatial scale of 100–400 km. Besides scatterometry wind vector data used in this study, microwave altimeter, synthetic aperture radar, and microwave radiometer also measure ocean surface wind speed [*Sikora et al.*, 1995; *Kudryavtsev et al.*, 1996; *Beal et al.*, 1997; *Liu*, 2002] with complementary coverage (spatial and temporal) as well as resolution to scatterometer. The incorporation of these sensors will be useful in further investigations.

[12] **Acknowledgments.** The authors wish to thank Drs. Norden Huang and Antony Liu of the NASA Goddard Space Flight Center for helpful discussions. This study is funded by the National Science Council of Taiwan (Projects: National Center for Clean Research and NSC 91-2119-M-002-032).

References

Beal, R. C., et al., The influence of the marine atmospheric boundary layer on ERS 1 synthetic aperture radar imagery of the Gulf Stream, *J. Geophys. Res.*, *102*, 5799–5814, 1997.

Chang, S. W., and R. A. Anthes, Numerical Simulations of the ocean's nonlinear baroclinic response to translating hurricanes, *Journal of Physical Oceanography*, *8*, 468–480, 1978.

Chelton, D. B., et al., Observations of coupling between surface wind stress and sea surface temperature in the Eastern Tropical Pacific, *Journal of Climate*, *14*, 1470–1498, 2001.

Chu, P. C., et al., Temporal and spatial variabilities of the South China Sea surface temperature anomaly, *J. Geophys. Res.*, *102*(C9), 20,937–20,955, 1997.

Emanuel, K. A., An air-sea interaction theory for tropical cyclones Part I, *Journal of Atmospheric Sciences*, *42*, 1062–1071, 1986.

Kudryavtsev, V. N., et al., Observations of atmospheric boundary layer evolution above the Gulf Stream frontal zone, *Boundary Layer Meteorology*, *79*, 51–82, 1996.

Leipper, D. F., Observed ocean conditions and hurricane Hilda, *Journal of Atmospheric Science*, *24*, 182–196, 1967.

Lin, I., et al., Observations of typhoon-induced upper ocean cooling in the Western Pacific Ocean by cloud penetrating remote sensor, in preparation.

Liu, W. T., et al., Atmospheric manifestation of tropical instability wave observed by QuikSCAT and Tropical Rain Measuring Mission, *J. Geophys. Res. Lett*, *27*(16), 2545–2548, 2000.

Liu, W. T., Satellite remote sensing: Wind, surface, *Encyclopedia of Atmospheric Sciences*, Academic Press, London, in press, 2002.

Monaldo, F. M., et al., Satellite imagery of sea surface temperature cooling in the wake of hurricane Edouard (1996), *Monthly Weather Review*, *125*, 2716–2721, 1997.

Nelson, N. B., The wake of hurricane Felix, *International Journal of Remote Sensing*, *17*(15), 2893–2895, 1996.

Price, J. F., Upper ocean response to a hurricane, *Journal of Physical Oceanography*, *11*, 153–175, 1981.

Sikora, T. D., et al., Use of ERS-1 synthetic aperture radar imagery of the sea surface in detecting the presence and structure of the convective marine atmospheric boundary layer, *Monthly Weather Review*, *123*, 3623–3632, 1995.

Wallace, J. M., et al., The influence of sea surface temperature on surface wind in the eastern equatorial Pacific: Seasonal and interannual variability, *Journal of Climate*, *2*, 1492–1499, 1989.

Wentz, F. J., et al., Satellite measurements of sea surface temperature through clouds, *Science*, *288*, 847–850, 2000.

Xie, S. P., et al., Coupled ocean-atmospheric waves on the equatorial front, *J. Geophys. Res. Lett.*, *25*, 3863–3966, 1998.

Xie, S. P., et al., Far-reaching effects of the Hawaiian Islands on the Pacific ocean-atmosphere system, *Science*, 292, 2001.

I.-I. Lin, National Center for Ocean Research, P.O. Box 23-13, Taipei 10617, Taiwan. (linii@odb03.ncor.ntu.edu.tw)

W. T. Liu, Jet Propulsion Laboratory, NASA, USA. (liu@pacific.jpl.nasa.gov)

C.-C. Wu, Department of Atmospheric Sciences, National Taiwan University, Taiwan. (cwu@typhoon.as.ntu.edu.tw)

J. C. H. Chiang, Joint Institute for the Study of the Atmosphere and Ocean, University of Washington, USA. (jchiang@atmos.washington.edu)

C.-C. Sui, Institute of Hydrological Sciences, National Central University, Taiwan. (sui@cc.ncu.edu.tw)